IEEE Access
Multidisciplinary | Rapid Review | Open Access Journal

Received 22 July 2024, accepted 9 August 2024, date of publication 16 August 2024, date of current version 27 August 2024.

*Digital Object Identifier 10.1109/ACCESS.2024.3445330*

RESEARCH ARTICLE

# Earthworm-Inspired Robot Design: Reducing the Number of Actuators Through Embedded Motor Between Segments

**WILLIAM LEONARD LIEM[1], AYATO KANADA[2], (Member, IEEE), AND TOMOAKI MASHIMO[3], (Member, IEEE)**

[1]Department of Mechanical Engineering, Toyohashi University of Technology, Toyohashi 441-8580, Japan
[2]Department of Mechanical Engineering, Kyushu University, Fukuoka 819-0395, Japan
[3]Graduate School of Natural Science and Technology, Okayama University, Okayama 700-8530, Japan

Corresponding author: Ayato Kanada (kanada.ayato.853@m.kyushu-u.ac.jp)

This work was supported in part by the Japan Society for the Promotion of Science (JSPS) KAKENHI under Grant 22H01446.

**ABSTRACT** Typically, earthworm-inspired robots consist of N segments and N actuators, each segment having one actuator. However, to reduce the number of actuators, complex mechanisms are often required to activate multiple segments. In this study, we introduce a novel design for an earthworm-inspired robot that reduces the number of actuators from N to N-1, thereby simplifying the mechanical complexity while maintaining high performance. Our proposed robot consists of three segments and two motors embedded between the segments. These two motors share a single flexible shaft and move back and forth along it. By extending or retracting the segments through the movement of the motors, the robot is propelled forward. We evaluated the robot's performance, achieving a maximum speed of 11.6 mm/s, a payload capacity of 200 g (three times its own weight), and a climbing angle of 20 degrees, demonstrating its superior capabilities in various scenarios. The proposed robot generates significant force through simultaneous motor actuation and exhibits effective steering locomotion with additional actuators. This study introduces a new design approach for earthworm-inspired robots and offers valuable insights into achieving locomotion with fewer actuators.

**INDEX TERMS** Earthworm robots, piezoelectric actuators, soft robots, ultrasonic motors.

## I. INTRODUCTION

Earthworm-inspired robots have garnered attention for their ability to efficiently navigate unstructured terrain in soft robotic applications such as search and rescue [1], [2], infrastructure inspection [3], [4], [5], medical endoscopy [6], [7], [8], and soil drilling [9], [10], [11], [12]. These robots typically have a segmented body with one actuator in each segment, resulting in N segments requiring N actuators [13]. Previous attempts to reduce the number of actuators have led to complex mechanisms and non-reversible motions [14], [15], [16], [17]. We present a simple earthworm-inspired robot design that operates with N-1 actuators to address this issue.

The associate editor coordinating the review of this manuscript and approving it for publication was Tao Wang.

Peristaltic motion, a pattern of movement produced by a sequence of deformations in three or more serially connected segments, propels earthworm-inspired robots [18], [19]. This pattern is typically generated by using an equal or greater number of actuators as there are segments. Actuators located within the segments produce radial expansion and axial contraction to drive the robot. To reduce the number of actuators, one actuator should be able to actuate multiple segments. Boxerbaum et al. developed a cylindrical robot with a braided mesh body wrapped with steel cables that can be driven by a single motor using a cam mechanism to pull multiple cables [14]. This mechanism can produce a continuous wave of peristalsis for locomotion but requires a large number of specialized joints to secure the mesh and cables. Glozman et al. developed a pneumatic earthworm-inspired robot controlled by a single air supply

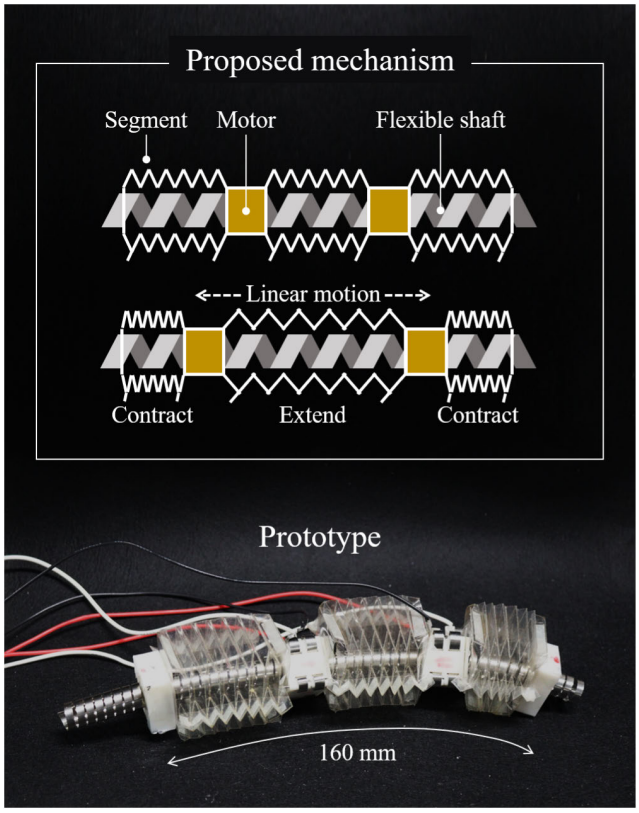


**FIGURE 1. Concept of the proposed earthworm-inspired robot with fewer actuators. This robot consists of three segments and two motors embedded between the segments.**

channel [15]. This robot generates peristaltic motion by controlling the expansion time of each balloon segment through varying orifice diameters. While this simple system eliminates the need for actuators within the robot, it cannot generate reverse motion. Sato et al. developed a new pneumatic valve controlled by the rotary motion of a single motor [20]. The valve has a single supply source and sequentially activates multiple balloon segments to generate peristaltic motion. Reverse motion would be possible by changing the direction of rotation of the motor, but the system is relatively complex due to the need for tubing between segments. As a locomotion similar to peristaltic motion, inchworm motion for mobile robots with few motors has also been studied [21], [22]. However, inchworm robots and earthworm robots are essentially different in terms of their locomotion mechanism [23].

In this study, we propose a new design for an earthworm-inspired robot that reduces the number of actuators. As shown in Fig. 1, our robot consists of three segments and two motors placed between the segments. The two motors share a single flexible shaft and move back and forth along the shaft. The movement of the motors extends or retracts the segments, thereby propelling the robot. Although the individual segment lengths vary during locomotion, the total segment length is always constant, determined by the length of the flexible shaft. The flexible shaft can be designed to be hollow. This design reduces the number of actuators (motors) by placing them between the segments instead of on each segment. Additionally, this design offers two advantages. Firstly, it allows for the generation of a large force. The multiple motors can operate simultaneously to provide a large force to the shared single shaft. Secondly, it allows for easy insertion of additional sensors, actuators, and cameras into the flexible shaft. The flexible shaft has a constant length, even while the robot is moving, making it easy to install such additional systems inside it.

To achieve the proposed mechanism, we have developed a flexible ultrasonic motor (FUSM) as part of the innovation that enables the reduced number of actuators in the new design [24]. This motor consists of a metallic cubic part that has a through-hole, into which a coil spring shaft is inserted. When applying voltages, the metallic part slides on the coil spring that works as the flexible shaft. Unlike a rigid shaft, the coil spring can provide a tortuous path for the metallic part, which can be applied to soft robots.

The remainder of this article is structured as follows. In Section II, we explain the driving principle behind the FUSM and present a prototype design of the earthworm-inspired robot. Section III evaluates key performance metrics such as thrust force, speed, payload, and climbing ability. Additionally, we demonstrate steering locomotion by incorporating other actuators into the coil spring. Finally, in Section IV, we conclude this article.

## II. FLEXIBLE ULTRASONIC MOTOR

### A. DRIVING PRINCIPLE

Let us explain the driving principle of the flexible ultrasonic motor briefly [24]. This motor is a type of piezoelectric actuator and is driven by the vibration of piezoelectric elements. Two piezoelectric plates are adhered on the sides of the metallic part with a through hole for the coil spring shaft, as shown in Fig. 2(a). To move on the coil spring linearly, the metallic part excites two vibration modes simultaneously. We call the two vibration modes T1 and T2 modes for translation. Fig. 2(b) shows how these vibration modes vibrate. The T1 mode is a vibration that repeats expansion and contraction symmetrically. The T2 mode is a vibration that expands the metallic part edge asymmetrically about the axial direction. Both modes are excited simultaneously when two voltages are applied to the piezoelectric plates. These voltages are expressed as

$$\begin{aligned} E_1 &= A_E(\sin(2\pi f_E t)) \\ E_2 &= A_E(\sin(2\pi f_E t + \phi)) \end{aligned} \tag{1}$$

where $A_E$ and $f_E$ are the amplitude and frequency of the voltages, respectively, and $\phi$ is the phase between the two voltages. The metallic part moves forward when the phase $\phi$ is set to $-\pi/2$, and backward when $\phi$ is $\pi/2$.

In this paper, we use FUSMs developed in our previous work [24]. The metallic cube made of phosphor bronze has a side length of 14 mm, a center hole of 10 mm in diameter, and

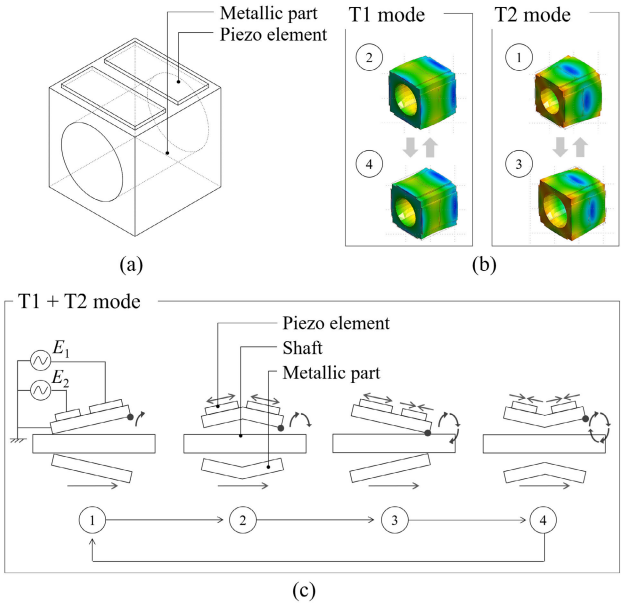


**FIGURE 2.** Driving principle of the flexible ultrasonic motors. (a) Schematic of the motor. (b) Two vibration modes (Mode 1 and Mode 2) are generated by a metallic part and an elliptical motion. (c) Applied voltages for the motor. Reproduced from [24].

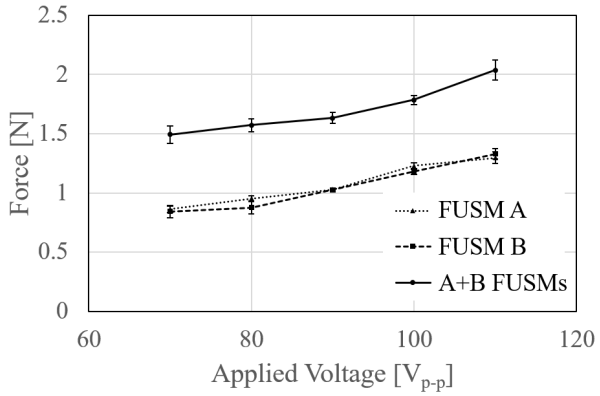


**FIGURE 3.** Relationship between the applied voltage and force of single FUSM and A + B FUSMs. The error bars show the standard deviations of five experiments.

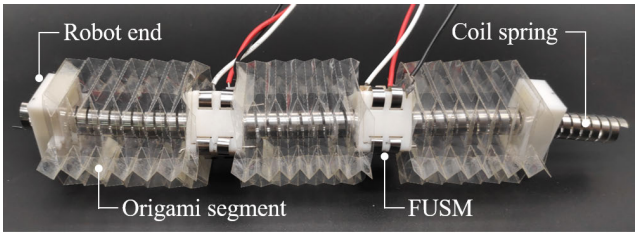


**FIGURE 4.** Prototype of the earthworm-inspired robot.

eight piezo elements adhered on the sides. The piezoelectric elements have a length of 14 mm, a width of 10 mm, and a thickness of 0.5 mm. The coil spring, which is a flat wire formed into a helix, has a diameter of 10.2 mm, a width of 3 mm, and a thickness of 0.15 mm. The metallic cube generates the thrust force for moving along the coil spring when $f_E = 82.0$ kHz.

### B. PRE-PRESSURE PRINCIPLE

Multiple FUSMs can generate a combined force on the shared single coil spring. Here we consider the effect of the shared coil spring on the output of the FUSMs. The most important parameter in determining the output is the pre-pressure between the metallic cube and the coil spring. The coil spring has a slightly larger diameter than the hole in the cube/FUSM and acts as a pre-pressure mechanism to improve the motor output. When the coil spring is inserted into the hole, the shrunken coil generates a pre-pressure $P$ at the interface between the hole and the coil spring. The pre-pressure $P$ can be expressed (see [24] for more details) using the coil's Young's modulus $E$, the coil thickness $h$, the coil radius $r_1$, and the hole radius $r_2$ as follows

$$P = \frac{Eh^3(r_1 - r_2)}{12{r_1}^2{r_2}^2} \tag{2}$$

The FUSM can generate a force proportional to the magnitude of $P$.

The coil spring with radius $r_1$ is inserted into the hole with radius $r_2$ and therefore has a radius between $r_1$ and $r_2$ near the hole. If the coil spring with a radius between $r_1$ and $r_2$ is inserted in the second and subsequent cubes, the pre-pressure exerted by this coil will be slightly less, reducing the output. However, this effect would be negligible in this study because the values of $r_1$ and $r_2$ are 5.1 mm and 5.0 mm respectively, a difference of only 0.1 mm; the coil spring returns to radius $r_1$ immediately in the vicinity of the hole.

### C. MOTOR PERFORMANCE

To confirm the increase in output by using multiple FUSMs, we prepare two FUSMs and make a comparison between the force generated by one FUSM alone and the force generated by two FUSMs connected in series. The force is measured by a force gauge attached to the end of the coil spring when changing the applied voltages $A_E$ from 70 $V_{p-p}$ to 110 $V_{p-p}$.

Fig. 3 shows that the force generated by both FUSMs simultaneously is approximately 50% - 80% higher than that generated by one FUSM. This feature is advantageous for robots with multiple segments, such as earthworm-inspired robots, which allow a specific segment to generate a large force. The reason why the force does not reach double with two FUSMs is probably because the FUSMs are not perfectly synchronized.

## III. EARTHWORM-INSPIRED ROBOT

### A. OVERVIEW

We build an earthworm-inspired robot using flexible ultrasonic motors, as shown in Fig. 4. This robot consists of a single coil spring, two FUSMs, two robot ends, and three origami segments. The single coil spring is inserted

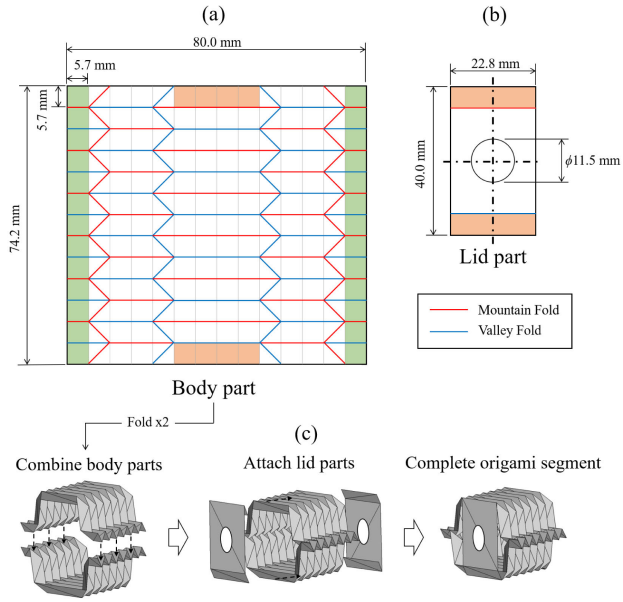


**FIGURE 5.** How to assemble origami segments. The origami segment consists of (a) a body part and (b) a lid part. (c) These two components are combined to build the origami segment.

into the two FUSMs, and its ends are fixed to the robot ends. The two FUSMs move linearly on the coil spring. The origami segments are glued between the first FUSM and the second FUSM or between a FUSM and a robot end. As the FUSMs move, the origami segments either extend or contract. Controlling the expansion and contraction of the segments can produce a peristaltic motion, propelling the robot. The prototype robot is 160 mm long and weighs 65 g.

### B. ORIGAMI SEGMENT

Let us explain the assembly process of the origami segment. The origami segment is composed of body parts and lid parts, which are made from PET films (Lumirror T60) and cut using laser machining, as shown in Fig. 5(a) and (b). We use a body part design known as the Tachi-Miura Polyhedron (TMP) [25], [26]. The folding pattern is made up of 14 × 13 square grids, with each grid measuring 5.7 mm. The red and blue lines represent the mountain and valley folds, respectively, while the thin gray lines indicate the grids on the pattern. Folding this pattern creates half of a bellow structure with an Omega-shaped cross-section, as shown in Fig. 5(c). Combining two of these patterns forms the bellows structure. The lid part is a simple rectangle with a hole in the center, through which the FUSM's coil spring can pass. The two lid parts are attached to the bellows structure to complete the origami segment.

Fig. 6(a) shows a prototype of the origami segment. The lid part of the origami segment has adhesive to attach the FUSM and the end holder. The origami segment has claws, which are made of U-shaped fasteners used in common staplers, on the bottom side, as shown in Fig. 6(b). The claws can anchor the segment to the ground to provide propulsion.

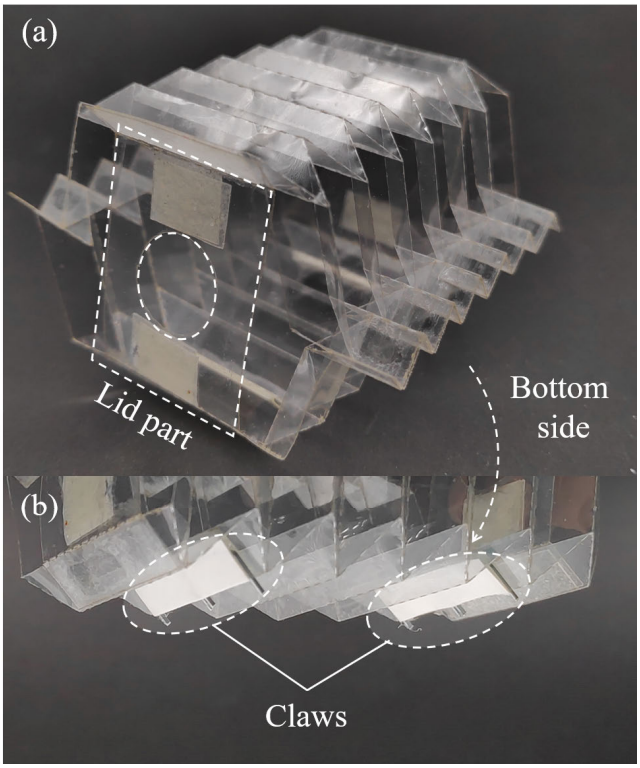


**FIGURE 6.** (a) Assembled origami segment. (b) Claws made of staples are attached to the bottom side of the origami segment (circled in white).

### C. LOCOMOTION CYCLE

The locomotion of the robot follows a 3-state cycle, which is illustrated in Fig. 7(a). In state 1, the front and rear segments of the robot are contracted, while the middle segment is extended. The contracted segment is anchored to the ground by the claw. To transition from state 1 to state 2, the rear FUSM moves forward. This action releases the rear anchor point and forms the middle anchor point. In state 2, the front and middle segments are contracted, while the rear segment is extended. To transition from state 2 to state 3, the front and rear FUSMs move backward simultaneously. This movement releases the front anchor point and forms the middle and rear anchor points. In state 3, the rear segment is contracted, and the front segment is extended. To transition from state 3 back to state 1, the front FUSM moves forward. This action releases the middle anchor point and forms the front anchor point, completing one stride of the locomotion procedure. This sequence propels the robot by a length $\Delta x$, which can be expressed as

$$\Delta x = L - 2\,d - 3L_{min} \tag{3}$$

where $L$ is the length of the entire robot without the robot ends, $d$ is the length of the FUSM, and $L_{min}$ is the minimum length of the segment. In the prototype robot, these parameters are given as follows: $L = 140$ mm, $d = 17.5$ mm, and $L_{min} = 20$ mm. Thus, the maximum distance advanced in one cycle is theoretically 45 mm. Fig. 7(b) shows the

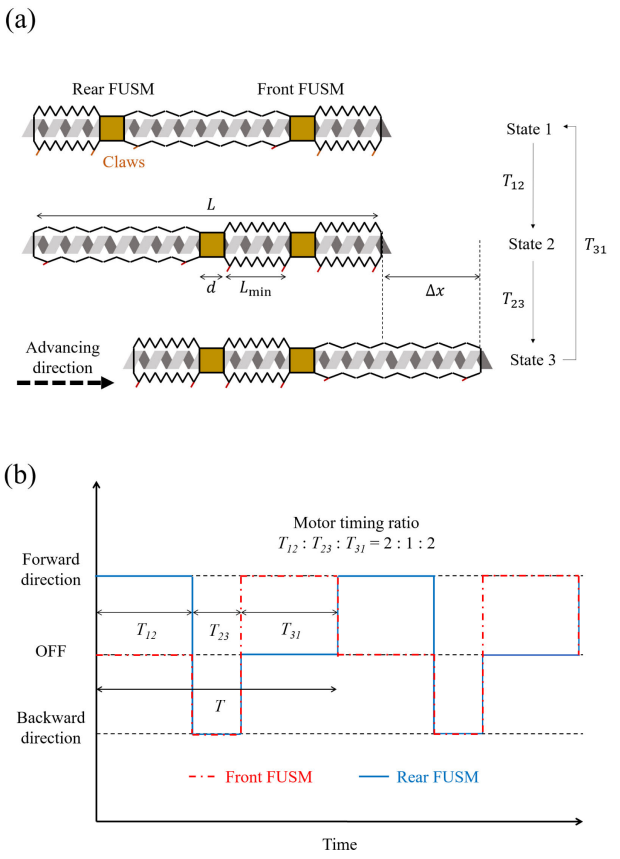


**FIGURE 7.** (a) Locomotion of the robot follows a 3-state cycle. (b) Direction of each of the motor movements during the locomotion.

sequence of signals applied to each motor to achieve the locomotion steps explained above. The direction of the signal indicates the movement direction of the motor relative to the coil spring. $T_{ij}$ indicates the timing of the signal in which the motor is driven during the state transition, where $i, j = 1, 2, 3$ and $i \neq j$. We set the timing ratio of the motor to be 2:1:2 for $T_{12}$, $T_{23}$ and $T_{31}$, respectively. The reason why $T_{23}$ is shorter than the others is that both motors run simultaneously, which allows for faster switching between states. The time of one cycle of locomotion is $T = T_{12} + T_{23} + T_{31}$. From (3), the robot's movement speed $v$ can be written as follows

$$v = \frac{\Delta x}{T}. \tag{4}$$

## IV. EXPERIMENTS

We evaluate the basic performance measures of the prototype robot, including frequency response, load-speed relationship, slope climbing, and turning. In the following experiments, the robot is operated on a flat surface covered by a thin layer of non-woven fabric. We set the amplitude and frequency of the voltage applied to the motors at 110 $V_{p-p}$ and 82 kHz, respectively. The performance results are summarized in Table 1.

**TABLE 1.** Performance results.

| Speed [mm/s] | Payload [g] | Climbing Angle [deg] | Turning Radius [mm] |
|---|---|---|---|
| 11.6 | 200 | 20 | 255 |

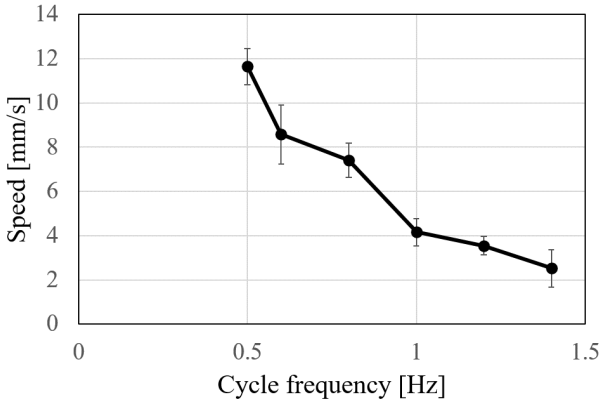


**FIGURE 8.** Relationship between the frequency of the locomotion cycle and the speed of the robot. The error bars show the standard deviations of five experiments.

### A. CYCLE FREQUENCY

We investigate how the cycle frequency of the locomotion affects the robot's speed. We measure the robot speed when changing the cycle frequency $T^{-1}$ from 0.5 Hz to 1.4 Hz. The lower limit was set to a time sufficient for the FUSM to fully extend or contract the segments.

Fig. 8 shows that the robot speed reaches a maximum value of 11.6 mm/s at the cycle frequency of 0.5 Hz, which is about half of the theoretical maximum speed calculated from (3) and (4). This difference occurs because the theoretical equation does not account for robot slippage or incomplete contraction of the segment. In addition, the robot's speed gradually decreases with increasing the cycle frequency. This is because, with higher frequencies, the contraction and expansion distance of the segment becomes shorter. The angle change of the claws attached to the bottom of the segment depends on this contraction and expansion distance. When the contraction and expansion distance is small, the claws cannot anchor sufficiently to the ground, resulting in a decrease in the robot's speed. In subsequent experiments, the cycle frequency was set to 0.5 Hz.

### B. LOAD-SPEED MEASUREMENT

Since one of the main specifications for mobile robots is their payload capacity, we investigate the relationship between the payload and the speed of the proposed robot. The rear end of the robot is connected to a tray for mounting weights as shown in Fig. 9. The bottom side of the tray is covered with ultra-high-molecular-weight polyethylene tape (commonly known as slick surface tape) to reduce the friction between the ground and the tray. The load on the robot is varied by

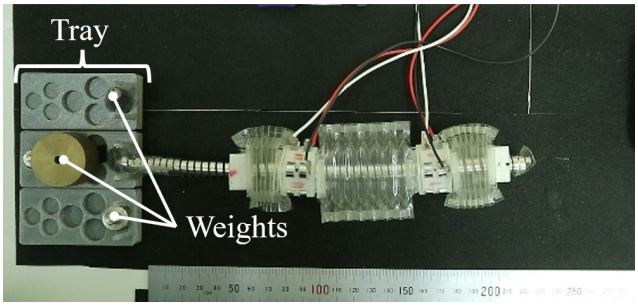


**FIGURE 9.** Experimental setup for Load-Speed measurement. The robot pulls a tray mounted with weights.

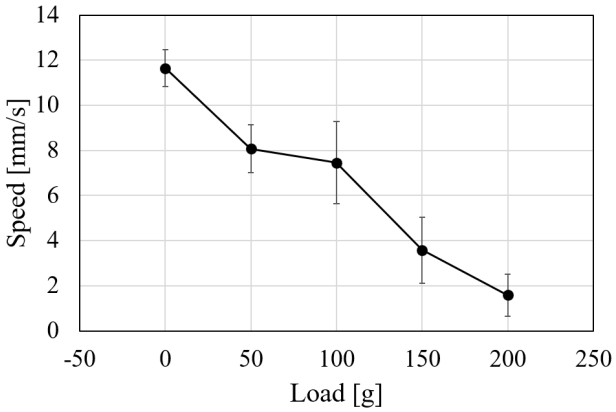


**FIGURE 10.** Relationship between the load pulled by the robot and the speed of the robot. The error bars show the standard deviations of five experiments.

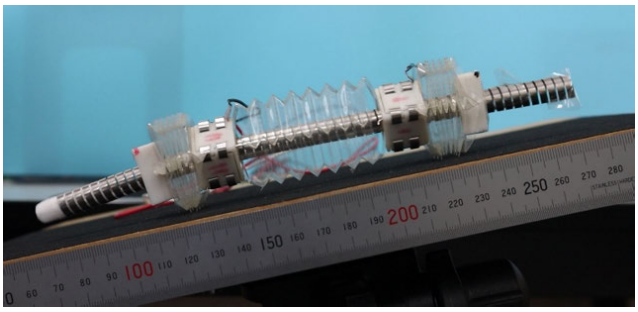

**FIGURE 11.** Experimental setup to measure the speed of the robot when climbing a slope. The robot climbs the slope at variable angles.

placing weights on the tray. When the load is set to 0 g, the tray is removed from the robot.

Fig. 10 shows the relationship between the load and the speed of the robot. The speed decreases as the load increases, and the robot can generate little or no motion when the load exceeds 200 g. The robot is capable of carrying a load of up to three times its weight at maximum.

### C. SLOPE CLIMBING

We investigate how far up the slope the robot can climb. Fig. 11 shows the experimental setup for slope climbing.

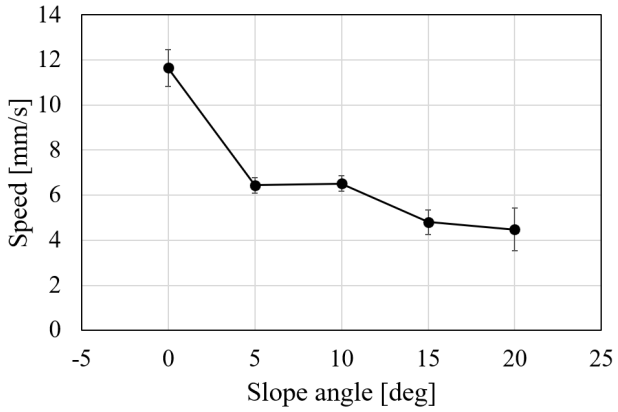


**FIGURE 12.** Relationship between the slope angle and the speed of the robot. The error bars show the standard deviations of five experiments.

The slope can be angled in 5-degree increments. We measure the robot's speed by increasing the angle of the slope from 0 degrees until the robot stops moving.

Fig. 12 shows the relationship between the slope angle and the robot speed. We observe that as the slope angle increases, the robot speed decreases. We also observe that the robot is unable to climb the slope at an angle of 25 degrees. As the angle of the slope increases, the weight force component of the robot perpendicular to the slope surface decreases. This reduction in the weight force leads to a decrease in the friction force between the slope surface and the claws, thereby causing insufficient grip on the slope surface. As a result, the robot experiences slipping during locomotion, leading to a decrease in its speed.

### D. TURNING

Earthworm-inspired robots change their overall length as their segments expand and contract, so the devices and sensors they use must be stretchable. However, stretchable systems are often less reliable and durable than those that are not. Our proposed constant-length robot can overcome this problem.

To illustrate this advantage, we demonstrate the turning motion of the robot using a non-stretchable bending device. This bending device is a type of continuum manipulator, featuring a central flexible tube actuated by sets of wires running along it, as shown in the top of Fig. 13. The wires are pulled by a motor at the end of the tube via a pulley to bend the device. We inserted this device into the hollow coil spring of the FUSM and secured its end to the coil's end with adhesive. As the bending device is activated, the robot body bends in an arc. When the robot in this state propels, the movement path is in an arc, as shown in the bottom of Fig. 13. Fig. 14 shows the traveling distance of the robot while turning. The robot advanced 140 mm and rotated 31.4 degrees in 30 seconds. This movement speed is about 1/3 that of the speed when the robot is straight. The reduction in movement speed is due to the increased friction caused by the disparate

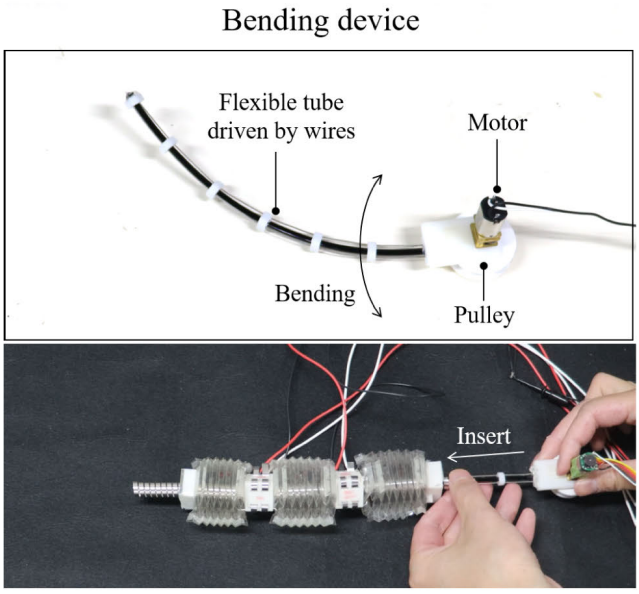


**FIGURE 13.** Turning motion of the robot with bending device. The proposed robot has a constant overall length, even when moving, allowing for easy insertion of external devices.

orientation of the claws. This experiment demonstrated that our robot is capable of embedding non-stretchable common external devices, which can help improve its performance.

## V. DISCUSSION

We compare the performance of our earthworm-inspired robot relative to other similar robots, as detailed in Table 2. Note that parameters marked with an asterisk are estimated based on images of reference papers. Our robot,

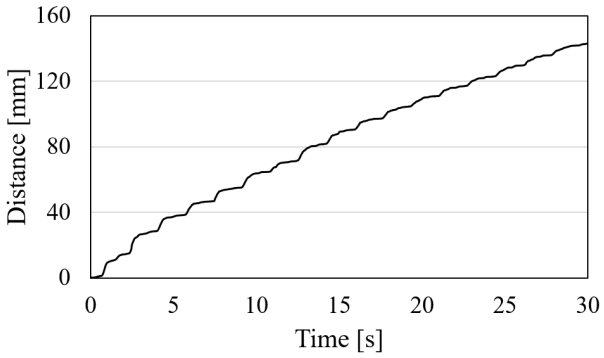


**FIGURE 14.** Travelling displacement of the robot in turning motion.

which employs flexible ultrasonic motors (FUSMs), exhibits significant advantages in terms of actuator volume and overall performance. Notably, our robot is very lightweight, weighing 65g for a length of 165mm, and uses only two actuators, each with a volume of $7.7 \times 10^3$ $mm^3$. This compact actuator volume contributes to simplified design, reduced weight, and increased travel speed. For instance, the pneumatic-driven robot referenced in [11] uses five actuators with a substantially larger volume of $62.4 \times 10^3$ $mm^3$ each, resulting in a slower maximum speed of 0.5 mm/s despite its greater length of 350 mm. The wire-driven robot in [17] has a design similar to our robot that uses a single actuator to move multiple segments, but it uses an actuator with a large volume of $199.2 \times 10^3$ $mm^3$, losing design simplicity. The design combining pneumatic and SMA actuators in [27] achieves a higher speed of 22.2 mm/s but requires a complex system of 25 actuators. In contrast, our robot's design balances compactness and speed effectively, with its two FUSMs enabling a maximum speed of 11.6 mm/s. However, our robot exhibits relatively weak power compared to other designs. This could be improved by using more stators.

Our proposed design has advantages and disadvantages. Reducing the number of actuators contributes to a lighter robot but loses a variety of locomotion. For example, earthworm-inspired robots with many actuators can change locomotion patterns to optimize the robot's speed and payload [28]. Sharing one flexible shaft with multiple motors can generate a large combined force but increases the impact of motor failure. Failure of one motor inhibits the movement of several surrounding segments.

There are also problems specific to FUSMs. Shaft flexibility makes precise position control difficult. One way to improve controllability is to incorporate position sensors in the flexible shaft for feedback control [29]. FUSMs have a simple structure and small size but also suffer from the inherent drawbacks of ultrasonic motors, such as high voltage, unstable operation, and short life [30], [31]. However, our design is not specific to FUSMs but could be applied to other actuators that can comprise a set of a flexible shaft and linear motors. It may apply to motor-driven [32], wire-driven [33], and magnet-driven robots [34].

**TABLE 2. Comparision with other earthworm-inspired robots.**

| Ref. | Actuation | Robot Mass [g] | Robot Length [mm] | Number of Segments | Number of Actuators | Volume of One Actuator [$mm^3$] | Force [N] | Speed [mm/s] |
|---|---|---|---|---|---|---|---|---|
| Ours | FUSM | 65 | 160 | 3 | 2 | $7.7 \times 10^3$ | 2.0 | 11.6 |
| [11] | Pneumatic | - | 350 | 5 | 5 | $62.4^* \times 10^3$ | 40-50 | 0.5 |
| [17] | Wire | 225 | 246 | 3 | 1 | $199.2^* \times 10^3$ | 3.8 | - |
| [27] | Pneumatic + SMA | 332 | 410 | 5 | 5 + 20 | - | 4.4 | 22.2 |

## VI. CONCLUSION

We proposed an earthworm-inspired robot featuring a unique design that embeds motors between segments, thereby reducing the number of actuators typically needed for N segments from N to N-1. This design maintains the robot's overall length constant, even during propulsion. Our comprehensive experiments demonstrated that our robot achieved a maximum speed of 11.6 mm/s, a payload capacity of 200 g, and a climbing angle of 20 degrees. Using flexible ultrasonic motors (FUSMs) as embedded motors offered additional benefits, including generating a large combined force by multiple FUSMs and easily inserting additional sensors, actuators, and cameras. The FUSM demonstrated a force increase of 50% - 80% with adding one motor. The robot's hollow structure and fixed overall length facilitate the easy insertion of various external devices. The insertion of a bending device enabled the robot to propel while turning. A summary of our research is provided in the supplementary video.

Future work will focus on optimizing the synchronization of multiple FUSMs for improved propulsion and force generation. Analyzing the effects of different synchronization patterns on the robot's performance will help identify the most efficient configurations.

## REFERENCES


[1] M. P. Nemitz, P. Mihaylov, T. W. Barraclough, D. Ross, and A. A. Stokes, "Using voice coils to actuate modular soft robots: Wormbot, an example," *Soft Robot.*, vol. 3, no. 4, pp. 198–204, Dec. 2016.

[2] L. F. Muff, A. S. Mills, S. Riddle, V. Buclin, A. Roulin, H. J. Chiel, R. D. Quinn, C. Weder, and K. A. Daltorio, "Modular design of a polymer-bilayer-based mechanically compliant worm-like robot," *Adv. Mater.*, vol. 35, no. 18, May 2023, Art. no. 2210409.

[3] S. Even and Y. Ozkan-Aydin, "Locomotion and obstacle avoidance of a worm-like soft robot," 2023, *arXiv:2304.04301*.

[4] J. I. Dewapura, P. S. Hemachandra, T. Dananjaya, W. V. I. Awantha, A. T. Wanasinghe, A. L. Kulasekera, D. S. Chathuranga, and V. P. C. Dassanayake, "Design and development of a novel bio-inspired worm-type soft robot for in-pipe locomotion," in *Proc. 20th Int. Conf. Control, Autom. Syst. (ICCAS)*, Oct. 2020, pp. 586–591.

[5] F. Connolly, P. Polygerinos, C. J. Walsh, and K. Bertoldi, "Mechanical programming of soft actuators by varying fiber angle," *Soft Robot.*, vol. 2, no. 1, pp. 26–32, Mar. 2015.

[6] K. Wang, G. Yan, G. Ma, and D. Ye, "An earthworm-like robotic endoscope system for human intestine: Design, analysis, and experiment," *Ann. Biomed. Eng.*, vol. 37, no. 1, pp. 210–221, Jan. 2009.

[7] K. Suzumori, T. Hama, and T. Kanda, "New pneumatic rubber actuators to assist colonoscope insertion," in *Proc. IEEE Int. Conf. Robot. Autom.*, Sep. 2006, pp. 1824–1829.

[8] J. E. Bernth, A. Arezzo, and H. Liu, "A novel robotic meshworm with segment-bending anchoring for colonoscopy," *IEEE Robot. Autom. Lett.*, vol. 2, no. 3, pp. 1718–1724, Jul. 2017.

[9] H. Omori, T. Nakamura, T. Yada, T. Murakami, H. Nagai, and T. Kubota, "Excavation mechanism for a planetary underground explorer robot," in *Proc. ISR 41st Int. Symp. Robotics*, Jun. 2010, pp. 1–7.

[10] V. Consumi, L. Lindenroth, J. Merlin, D. Stoyanov, and A. Stilli, "Design and evaluation of the SoftSCREEN capsule for colonoscopy," *IEEE Robot. Autom. Lett.*, vol. 8, no. 3, pp. 1659–1666, Mar. 2023.

[11] R. Das, S. P. M. Babu, F. Visentin, S. Palagi, and B. Mazzolai, "An earthworm-like modular soft robot for locomotion in multi-terrain environments," *Sci. Rep.*, vol. 13, no. 1, p. 1571, Jan. 2023.

[12] K. Isaka, K. Tsumura, T. Watanabe, W. Toyama, M. Sugesawa, Y. Yamada, H. Yoshida, and T. Nakamura, "Development of underwater drilling robot based on earthworm locomotion," *IEEE Access*, vol. 7, pp. 103127–103141, 2019.

[13] J. Liu, P. Li, and S. Zuo, "Actuation and design innovations in earthworm-inspired soft robots: A review," *Frontiers Bioeng. Biotechnol.*, vol. 11, Feb. 2023, Art. no. 1088105.

[14] A. S. Boxerbaum, K. M. Shaw, H. J. Chiel, and R. D. Quinn, "Continuous wave peristaltic motion in a robot," *Int. J. Robot. Res.*, vol. 31, no. 3, pp. 302–318, Mar. 2012.

[15] D. Glozman, N. Hassidov, M. Senesh, and M. Shoham, "A self-propelled inflatable earthworm-like endoscope actuated by single supply line," *IEEE Trans. Biomed. Eng.*, vol. 57, no. 6, pp. 1264–1272, Jun. 2010.

[16] B. Kim, M. G. Lee, Y. P. Lee, Y. Kim, and G. Lee, "An earthworm-like micro robot using shape memory alloy actuator," *Sens. Actuators A, Phys.*, vol. 125, no. 2, pp. 429–437, Jan. 2006.

[17] B. Winstone, T. Pipe, C. Melhuish, M. Callaway, A. C. Etoundi, and S. Dogramadzi, "Single motor actuated peristaltic wave generator for a soft bodied worm robot," in *Proc. 6th IEEE Int. Conf. Biomed. Robot. Biomechatronics (BioRob)*, Jun. 2016, pp. 449–456.

[18] J. Gray and H. Lissmann, "Studies in animal locomotion: VII. Locomotory reflexes in the earthworm," *J. Experim. Biol.*, vol. 15, no. 4, pp. 506–517, 1938.

[19] P. Dario and C. A. Mosse, "Review of locomotion techniques for robotic colonoscopy," in *Proc. IEEE Int. Conf. Robot. Autom.*, vol. 1, Apr. 2003, pp. 1086–1091.

[20] H. Sato, K. Uchiyama, Y. Mano, F. Ito, S. Kurumaya, M. Okui, Y. Yamada, and T. Nakamura, "Development of a compact pneumatic valve using rotational motion for a pneumatically driven mobile robot with periodic motion in a pipe," *IEEE Access*, vol. 9, pp. 165271–165285, 2021.

[21] T. Yamamoto, M. Konyo, K. Tadakuma, and S. Tadokoro, "High-speed sliding-inchworm motion mechanism with expansion-type pneumatic hollow-shaft actuators for in-pipe inspections," *Mechatronics*, vol. 56, pp. 101–114, Dec. 2018.

[22] Q. Xie, S. Liu, and X. Ma, "Design of a novel inchworm in-pipe robot based on cam-linkage mechanism," *Adv. Mech. Eng.*, vol. 13, no. 9, Sep. 2021, Art. no. 168781402110451.

[23] G. Blewitt, D. Cheneler, J. Andrew, and S. Monk, "A review of worm-like pipe inspection robots: Research, trends and challenges," *Soft Sci.*, vol. 4, no. 2, pp. 1–23, Mar. 2024.

[24] A. Kanada and T. Mashimo, "Design and experiments of flexible ultrasonic motor using a coil spring slider," *IEEE/ASME Trans. Mechatronics*, vol. 25, no. 1, pp. 468–476, Feb. 2020.

[25] H. Yasuda, T. Yein, T. Tachi, K. Miura, and M. Taya, "Folding behaviour of Tachi–Miura polyhedron bellows," *Proc. Roy. Soc. A, Math., Phys. Eng. Sci.*, vol. 469, no. 2159, Nov. 2013, Art. no. 20130351, doi: 10.1098/rspa.2013.0351.
[26] J. Butler, J. Morgan, N. Pehrson, K. Tolman, T. Bateman, S. P. Magleby, and L. L. Howell, "Highly compressible origami bellows for harsh environments," in *Proc. Volume 5B, 40th Mech. Robot. Conf.*, Aug. 2016, pp. 12–24, doi: 10.1115/detc2016-59060.
[27] Q. Zhang, H. Fang, and J. Xu, "Yoshimura-origami based earthworm-like robot with 3-dimensional locomotion capability," *Frontiers Robot. AI*, vol. 8, Aug. 2021, Art. no. 738214.
[28] A. Kandhari, Y. Wang, H. J. Chiel, R. D. Quinn, and K. A. Daltorio, "An analysis of peristaltic locomotion for maximizing velocity or minimizing cost of transport of earthworm-like robots," *Soft Robot.*, vol. 8, no. 4, pp. 485–505, Aug. 2021.
[29] Y. Sato, A. Kanada, and T. Mashimo, "Self-sensing and feedback control for a twin coil spring-based flexible ultrasonic motor," *IEEE Robot. Autom. Lett.*, vol. 5, no. 4, pp. 5425–5431, Oct. 2020.
[30] T. Sashida and T. Kenjo, *An Introduction to Ultrasonic Motors*. Oxford, U.K.: Clarendon, 1993.
[31] K. Uchino, "Piezoelectric ultrasonic motors: Overview," *Smart Mater. Struct.*, vol. 7, no. 3, pp. 273–285, Jun. 1998.
[32] Y. Luo, N. Zhao, Y. Shen, and P. Li, "A rigid morphing mechanism enabled earthworm-like crawling robot," *J. Mech. Robot.*, vol. 15, no. 1, Feb. 2023, Art. no. 011008.
[33] X. Zhan, H. Fang, J. Xu, and K.-W. Wang, "Planar locomotion of earthworm-like metameric robots," *Int. J. Robot. Res.*, vol. 38, no. 14, pp. 1751–1774, Dec. 2019.
[34] S. Guo, Q. Yang, L. Bai, and Y. Zhao, "Development of multiple capsule robots in pipe," *Micromachines*, vol. 9, no. 6, p. 259, May 2018.

**WILLIAM LEONARD LIEM** received the M.S. degree in mechanical engineering from Toyohashi University of Technology, Aichi, Japan, in 2023.

**AYATO KANADA** (Member, IEEE) received the Ph.D. degree in mechanical engineering from Toyohashi University of Technology, Aichi, Japan, in 2020. He is currently an Assistant Professor with the Mechanical Engineering Department, Kyushu University, Fukuoka, Japan.

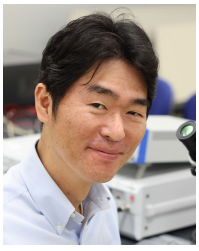

**TOMOAKI MASHIMO** (Member, IEEE) received the Ph.D. degree in mechanical engineering from Tokyo University of Agriculture and Technology, Tokyo, Japan, in 2008. He was a Robotics Researcher with the Robotics Institute, Carnegie Mellon University, Pittsburgh, PA, USA, from 2008 to 2010. After being an Assistant Professor (Tenure-Track) with Toyohashi University of Technology, Toyohashi, Japan, in 2011, he became an Associate Professor in 2016. Since 2022, he has been a Professor with the Graduate School of Natural Science and Technology, Okayama University. His research interests include piezoelectric actuators and robotic applications.